Advanced Ceramics Progress: Vol. 9, No. 3, (Summer 2023) 16-30

Materials and Energy Research Center
MERC

Contents lists available at ACERP

Advanced Ceramics Progress

Journal Homepage: www.acerp.ir

Original Research Article

Influence of B_4C Nanoparticles on Corrosion Characteristics of Ni Matrix Nanocomposite Coatings Fabricated via Pulse Electroplating Technique

Mohammad Kaveh [a], Mohammad Sajjadnejad [b*], Abbas Mohassel [b], Nader Setoudeh [c]

[a] *MSc, Department of Materials Engineering, School of Engineering, Yasouj University, Yasouj, Iran.*
[b] *Assistant Professor, Department of Materials Engineering, School of Engineering, Yasouj University, Yasouj, Iran.*
[c] *Associate Professor, Department of Materials Engineering, School of Engineering, Yasouj University, Yasouj, Iran.*

* Corresponding Author: m.sajjadnejad@yahoo.com; m.sajjadnejad@yu.ac.ir (Dr. Mohammad Sajjadnejad) URL: https://www.acerp.ir/article_206098.html

ARTICLE INFO

Article History:

Received: 06 December 2023
Revised: 09 April 2024
Accepted: 01 September 2024

Keywords:

Ni-B_4C Nanocomposite,
Pulse Electrodeposition,
Microstructure,
Corrosion,
Potentiodynamic Polarization

ABSTRACT

The Ni-B_4C nanocomposite coatings were fabricated via pulse electrodeposition on a copper substrate, and the effects of pulse current density, duty cycle, and pulse frequency on the microstructure, morphology, and corrosion characteristics were assessed. Field emission scanning electron microscopy (FESEM), energy-dispersive X-ray spectroscopy (EDS), X-ray diffraction (XRD), potentiodynamic polarization, and electrochemical impedance spectroscopy (EIS) tests were employed. The baseline electrodeposition conditions were set at i = 1 A/dm², γ = 50%, and f = 10 Hz. Embedding B_4C nanoparticles (NPs) into the nickel matrix significantly reduced the nickel crystallite size for the primary (111) and (200) crystal planes. Increasing the pulse current density from 1 to 4 A/dm² caused a substantial decrease in the incorporation rate of B_4C NPs, from 5.5 to 2.9 vol.%. However, an increase in the duty cycle from 25 to 50% and the pulse frequency from 1 to 10 Hz raised the incorporation rate to 5.5 vol.% and 4.6 to 3.9 vol.%, respectively. Surprisingly, the incorporation of B_4C led to an increase in the corrosion current density from 2.301 to 4.541 µA/cm². Increasing the pulse current density from 1 to 4 A/dm² and the duty cycle from 25 to 50% notably decreased the corrosion current density from 4.541 to 1.375 µA/cm² and from 7.243 to 4.541 µA/cm², respectively. Conversely, the minimum corrosion current density of 0.599 µA/cm², deposited at 1 Hz, increased significantly to 4.541 µA/cm² at 10 Hz, while the B_4C NPs content increased from 3.9 to 5.5 vol.%, possibly due to a more uniform distribution of B_4C NPs at 1 Hz. The Ni-B_4C specimen deposited at 1 Hz exhibited a higher Rct compared to the pure nickel sample under baseline conditions, indicating strong consistency between the EIS and potentiodynamic results.

https://doi.org/10.30501/acp.2024.429141.1141

1- INTRODUCTION

In recent years, coatings have been extensively applied to various substrates to significantly enhance surface characteristics such as mechanical properties, wettability, adhesion, lubrication, as well as scratch, wear, and corrosion resistance [1-4]. Several coating fabrication techniques have been utilized, including plasma spray [5], sol-gel [6-8], high-velocity oxygen fuel (HVOF) [9], chemical vapor deposition (CVD) [10], physical vapor deposition (PVD) [11], electrophoretic deposition [12] and electrodeposition [12-17], to improve surface and tribology as well as corrosion properties.

Electrodeposition is well known as a fundamental technique for fabricating metal matrix composite (MMC)

Please cite this article as: Kaveh, M., Sajjadnejad, M., Mohassel, A., Setoudeh, N. "Influence of B_4C nanoparticles on Corrosion Characteristics of Ni Matrix Nanocomposite Coatings Fabricated via Pulse Electroplating Technique", ***Advanced Ceramics Progress***, Vol. 9, No. 3, (2023), 16-30. https://doi.org/10.30501/acp.2024.429141.1141

coatings [18]. It is also regarded as one of the most efficient approaches, offering advantages such as easy preparation, versatility, and low cost for producing composite coatings based on both metallic and non-metallic components [19, 20]. These coatings are reinforced with second-phase particles, including ceramic carbides, oxides, nitrides, silicates, and diamond particles. Examples of these reinforcements include SiC [21, 22], B_4C [23-25], WC [26], TiO_2 [27, 28], Al_2O_3 [19, 29], ZnO [30, 31], Y_2O_3 [32], Ni_3S_4 [33], TiN [34, 35], graphene [36], CNT [32], and diamond [33], which help produce micro- and nanocomposite coatings with enhanced microhardness, texture, self-lubrication, wear resistance, tribological characteristics, and corrosion and oxidation resistance [1, 15, 16, 37].

Metal matrix composites (MMCs) are widely employed in material manufacturing. The metallic element forms the basis of the composite, while ceramic compounds act as second-phase reinforcing particles, defining the mechanical and structural properties. As one of the leading types of composite coatings, MMCs have widespread applications in various industries [12]. They are particularly well-known for their excellent wear, abrasion, corrosion, and high-temperature resistance, as well as their remarkable hardness, rigidity, stiffness, and modulus of elasticity [18].

Nickel and its alloys offer a wide range of applications in electrodeposited coatings due to their high strength-to-weight ratio, toughness, electrical and thermal conductivity, strong optical reflectivity, and, most notably, exceptional chemical stability and corrosion resistance. Nickel's tendency to form a protective passive layer contributes to the outstanding corrosion resistance of nickel matrix coatings in aqueous, saline, mineral acids, alkaline, and organic environments [15, 16, 38-41]. As a result, nickel matrix coatings are among the most extensively researched categories of MMC coatings, thanks to their protective nickel layer, excellent corrosion resistance, reproducibility, low cost, easy maintenance, and reduced energy requirements [42, 43]. Nickel matrix coatings reinforced with ceramic micro- and nanoparticles are widely used in various industries, including gears, bearings, blades, and the coal, petroleum, chemical, petrochemical (oil and natural gas), marine, automotive, medical, and aviation sectors (e.g., aircraft parts), offering superior microhardness, modulus of elasticity, wear, and corrosion resistance [12, 34, 44].

In recent years, nanoparticles have increasingly proven to be effective reinforcing agents in composite coatings, enhancing the mechanical, tribological, corrosion, and oxidation resistance properties compared to pure metal and micro-sized composite coatings [45]. The nanocomposite electrodeposition process occurs in at least three consecutive steps: i) transport of nanoparticles in the electrolyte toward the electrode, ii) absorption onto the surface of the electrode (cathode), and iii) embedment via the metallic particles of the electrodeposits [46].

Pulse electrodeposition (PE) is the preferred method for creating nickel-based coatings on blades, cylinders, bearings, and valves. PE offers several advantages, including ease of operation, high efficiency, safety, reliability, and lower cost compared to direct current (DC) electrodeposition, reverse PE, and brushing electrodeposition [47, 48]. For example, the use of PE in fabricating Ni–W/SiC nanocoatings via a modified Watt's nickel solution demonstrates excellent anti-corrosion performance in a 3.5 wt% NaCl corrosive environment [49]. PE provides precise control over the microstructure, mechanical properties, and corrosion resistance of electrodeposited coatings. Additionally, PE allows for a higher average current density (ia) compared to the DC method, preventing the formation of dendrites in the coating morphology. The participation of reinforcing particles is also significantly higher in the pulse current (PC) method than in the DC approach [17, 50]. The pulse electrodeposition parameters include current density (i), duty cycle (%), and pulse frequency ("γ"). These factors have a significant impact on the characteristics of PC electrodeposited coatings. The PC approach represents the duty cycle as the proportion of total on-time inside a pulse cycle, expressed as a percentage [51, 52]:

$$\text{Duty cycle } (\gamma) = \frac{T_{on}}{T_{on}+T_{off}} = T_{on}.f \quad (1)$$

where *f* is pulse frequency and is indicated as the cycle time (*T*) reciprocal [51, 52]:

$$\text{Frequency (f)} = \frac{1}{T_{on}+T_{off}} = \frac{1}{T} \quad (2)$$

The mean current density (I_A) formulated in the PC technique is also described as [51]:

$$I_A = \text{peak current } (I_p) \times \text{duty cycle } (\gamma) \quad (3)$$

The electrolyte conditions in the PC approach include factors such as bath chemical composition, temperature, pH, plating time, and stirring rate. Additionally, the characteristics of the incorporated particles—such as particle size, shape, concentration, dispersion type, and other surface properties—play an important role in determining the microstructure and morphology of the coatings [15, 16]. These factors, in turn, significantly influence the enhancement or reduction of the corrosion and wear resistance of the coatings [17, 23, 44].

A review of the literature reveals that B_4C in MMCs is regarded as an ideal reinforcing agent due to its outstanding mechanical properties and high chemical stability [53]. With a melting point of 2350°C and a Mohs hardness of 9.5, B_4C is one of the most stable materials, resistant to corrosion by hot hydrogen fluoride (HF) and nitric acid (HNO3), and insoluble in both acids and water [54]. In a very recent study conducted by Ramadoss et al. [55], an aluminum hybrid metal matrix composite (AHMMC) reinforced with B_4C and BN particles significantly improved corrosion resistance due to the formation of a protective layer. The incorporation of B_4C nanoparticles into Ni-B matrix composite coatings, fabricated via the electroless method, led to a remarkable increase in the microhardness and wear resistance of the Ni-B-B_4C composite coatings [56]. Pushpanathan et al. [57] studied the effect of varying pulse current density (up to 2 A/dm²) and duty cycle (up to 30%) for pulse-electrodeposited Ni-B_4C-TiC nanocomposite coatings under a fixed pulse frequency and nanoparticle concentrations of 0.5 g/L B_4C and 1 g/L TiC. The results showed improved hardness and wear resistance compared to the pure Ni-B coating. Similarly, the findings of [24] on Ni-B-based pulse electrodeposited composite coatings reinforced with B_4C sub-micron particles on N80 steel indicated an average microhardness of 1030.61 Hv and enhanced wear resistance with a coefficient of friction (COF) of 0.22. Additionally, the coatings exhibited good corrosion resistance, with a corrosion voltage of -0.3 V and a corrosion current of -1.15 μA for Ni-B/ B_4C coatings deposited at 2 g/L

in a 3.5 wt% NaCl solution. In another study, Dong et al. [58] fabricated superhydrophobic composite coatings on Q235 steel and found that the incorporation of B_4C particles created a unique micro-nano structure, inducing rough morphology, improving corrosion resistance, and promoting coating growth, resulting in a strong barrier effect and enhanced stability. Increasing the pulse frequency from 1 to 10, 100, and 1000 Hz in Ni-W-based coatings reinforced with B_4C nanoparticles revealed a significant reduction in grain size and roughness, a decrease in Ni content, and an increase in the participation of W and B_4C in the coating. The composite coating deposited at 100 Hz demonstrated the best corrosion resistance [59]. Optimizing electroplating parameters such as electrolyte bath temperature, deposition current intensity, and plating time, with the aid of Response Surface Methodology (RSM), can greatly enhance the hardness and corrosion resistance of electroplated Ni-B_4C coatings on AZ31 Mg alloy, demonstrating the effectiveness of Ni-B_4C composite coatings [60].

To the best of our knowledge, although other researchers have explored the effects of incorporating B_4C micro- and nanoparticles into metal matrix composites—particularly nickel-based coatings produced using various methods and deposition conditions—there have been few comprehensive studies on how the operating parameters of pulse electrodeposition (PE) influence the microstructure, texture, morphology, particle incorporation rate, and corrosion properties of these composite coatings. This study aims to develop nickel-based composite coatings strengthened with B_4C nanoparticles using the PE technique. The microstructure, morphology, and corrosion characteristics of the resulting Ni-B_4C coatings are evaluated through potentiodynamic polarization tests and electrochemical impedance spectroscopy. These coatings are deposited under varying pulse parameters, including pulse current density, duty cycle, and pulse frequency. The findings of this investigation are thoroughly analyzed and discussed.

2- MATERIALS AND METHODS

The nanocomposite coatings were electrodeposited onto a copper substrate in Watt's bath electrolyte. This section outlines the essential equipment and conditions required for the electrodeposition process, examines the influencing parameters, details the surface preparation, and describes the various tests used to assess the microstructural, morphological, and corrosion characteristics. These assessments were conducted using FESEM, EDS, XRD, potentiodynamic polarization, and EIS techniques.

2-1– THE PROCURATION OF ELECTRODEPOSITION BATH

In this research, the conventional electrolyte solution for fabricating nickel-based coatings, known as Watt's bath, was used. The main component of Watt's bath is nickel sulfate ($NiSO_4 \cdot 6H_2O$), which is employed to fabricate pure nickel and nickel nanocomposite coatings reinforced with B_4C nanoparticles. Nickel chloride ($NiCl_2 \cdot 6H_2O$) is then added to enhance the ionic conductivity of the solution. During electrodeposition (also known as electroplating), an external current is applied to the solution, promoting ion movement, improving electroplating efficiency, and reducing energy consumption.

An anionic surfactant, sodium dodecyl sulfate (SDS) with the chemical formula $CH_3(CH_2)_{11}SO_4Na$, is used as a surface activation agent to prevent particle agglomeration by increasing electrostatic repulsion. SDS also alters wettability, facilitates the uniform distribution of nanoparticles in the bath, and minimizes the porosity of the coating. The surface activation mechanism charges neutral particles and, with the help of the applied current, creates optimal conditions for particle incorporation into the matrix [61]. Finally, the boric acid (H_3BO_3) is added to the solution to control the pH of the bath. All chemical compounds were utilized as-received and were procured from Merck company. The electrodeposition bath composition, production company, and coordinated concentration are characterized in Table 1.

Table 1. The electrodeposition bath's chemical composition and concentration

Chemical composition	Concentration (g/L)
$NiSO_4.6H_2O$	300
$Na_3C_6H_5O_7$	40
B_4C	5
$CH_3(CH_2)_{11}SO_4Na$ (SDS)	40
NH_3	0.3

The TEM image and the corresponding specification of B_4C nano-powders utilized in this research are illustrated in Figure 1 and tabulated in Table 2, respectively.

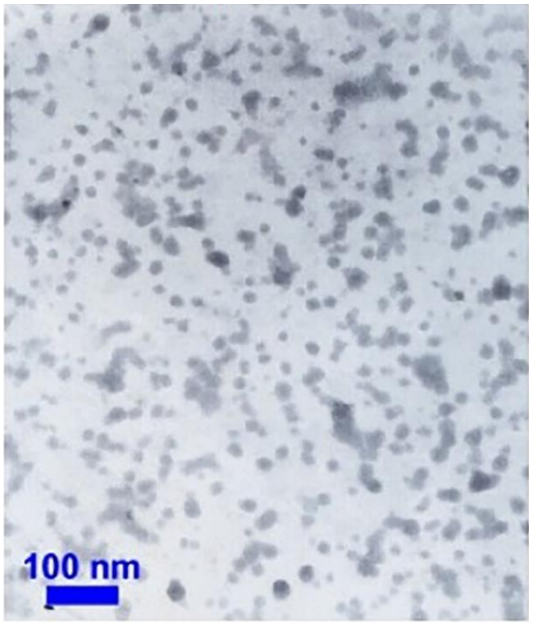

Figure 1. TEM image of B_4C nano-powders.

Table 2. The specification of B_4C nano-powders

Product Name	Boron Carbide Nanopowder (g/L)
Purity	99.0 %+
Dissociate Oxygen Content	0.8
Crystaline Phase	Monocrystalline
Particle Size	<50nm
Specific Surface Area	75 m^2/g
Loose Loading Density	0.01 g/cm^3
Color	Grey Black

2-2 – PREPARATION OF THE SUBSTRATE

To prepare the coating specimens, copper was selected as the substrate, and several samples were cut to achieve a uniform surface area. The copper substrates were ground using SiC abrasive paper from 150 to 2000 grit, then polished with alumina slurry solution (mean particle size of 1 μm) to achieve a mirror-like finish. The samples were cleaned with acetone under ultrasonication, immersed in a 15% HCl dilute solution for surface activation, and slightly corroded at the grain boundaries to enhance coating adhesion. Finally, the samples were rinsed in distilled water and absolute alcohol, dried with hot air, and made ready for use in the three-electrode electrodeposition cell.

2-3 – THE PROCESS OF ELECTRODEPOSITION

The electrodeposition bath was prepared according to the instructions detailed in Section 2-1 and poured into a 50 mL beaker. The solution was then stirred using a magnetic heater and preheated to ensure even distribution. Prior to preheating, the required amount of B_4C nanoparticles was added to the Ni-B_4C electrodeposition bath. To prevent nanoparticle agglomeration and ensure their suspension in the electrolyte, SDS was also added to the bath. The solution was stirred for 24 hours to hydrate the nanoparticles and improve their wettability. A temperature controller was used to maintain the bath temperature. The electrodeposition parameters are summarized in Table 3.

Table 3. The electrodeposition bath parameters

Electrodeposition bath parameter	Value /Degree
pH	4
Temperature (°C)	50
Stirring rate (rpm)	250

In this study, five separate specimens were prepared based ib variant electrodeposition parameters, as provided in Table 4.

Table 4. Pulse electrodeposition parameters of pure nickel and nickel-B_4C nanocomposite coating samples under variant electrodeposition conditions

Sample	B_4C nanoparticle concentration (g/l)	Maximum Current density (i_p) (A/dm^2)	Duty cycle (%)	Pulse frequency (Hz)
*Ni- B_4C (Baseline Ni -B_4C)	5	1	50	1
Ni- B_4C	5	4	50	1
Ni- B_4C	5	1	25	1
Ni- B_4C	5	1	50	10
Pure nickel (Baseline Ni)	-	1	50	1

* Baseline sample

The substrate surface area must be precisely defined for electrodeposition. To achieve this, the area not intended for coating must be insulated from contact with the electrolyte using electrical (friction) tape or nail lacquer. Just before starting the electrodeposition process, the electrolyte bath (solution) was subjected to ultrasonication to disperse all particles evenly. The electrodeposition cell was then partially immersed in the electrolyte solution, and the sample was placed into the cavity of the cell. The electrolyte was stirred at a maximum velocity of 250 rpm.

For electrodeposition, nickel served as the anode and copper as the cathode. The anode-to-cathode surface area ratio was maintained between 3 to 5 to prevent anodic polarization, and the distance between them was set to 2 to 3 cm. Pulse frequency, duty cycle, total time (T_{ON} + T_{OFF}), and On and Off times of the electrodeposition process were calculated separately to determine the required current based on the desired current density. Unlike direct current (DC) electrodeposition, pulse current (PC) electrodeposition used a conventional power supply with a current converter to produce a pulse current. The negative (-) and positive (+) poles of the power supply were connected to the cathode and anode, respectively, via electric wires to the pulse generator of the power supply.

After electrodeposition, the specimens were carefully removed from the electrolyte solution without direct hand contact and immediately immersed in distilled water, followed by ultrasonication for a brief period. This process helps to detach particles with weak bonds from the surface, improving the accuracy of subsequent analyses. After drying, the characteristics of the coated nanocomposite samples were examined using FESEM, XRD, and corrosion tests.

2-4 – ELECTROCHEMICAL CORROSION TESTS

The pure nickel and nickel-B_4C nanocomposite coating specimens were prepared for electrochemical corrosion tests. First, each coating sample was pierced with a tiny drill, connected to an electric wire, and the surrounding excess surfaces were insulated with lacquer. Following sample preparation, potentiodynamic polarization tests were conducted. The experiments were performed in a Pyrex glass three-electrode cell, with a 3.5 wt.% NaCl solution as the corrosive electrolyte. All tests were carried out at room temperature. Prior to testing, each specimen was immersed in the corrosive solution for 45 minutes to allow the surface to reach equilibrium with the corrosive components in the electrolyte. The corrosion measurements were conducted using an AUTOLAB PGSTAT-302N instrument equipped with NOVA 2.1.4 software for potentiodynamic polarization tests. The various components of the AUTOLAB PGSTAT-302N instrument, the corrosion test cell setup, and the pure nickel and Ni-B_4C coating specimens are clearly illustrated in Figures 2 and 3.

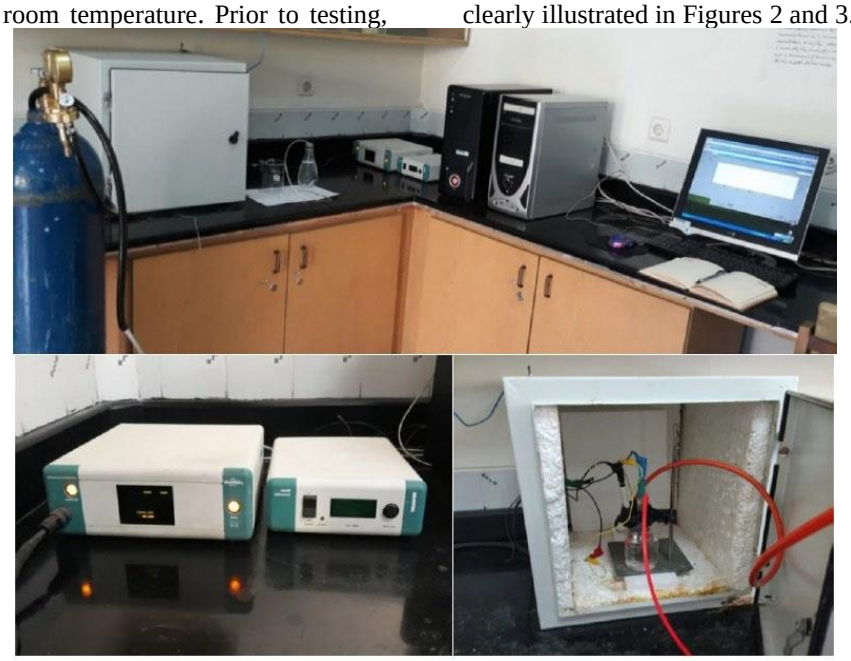

Figure 2. The AUTOLAB PGSTAT-302N instrument and corrosion cell setup.

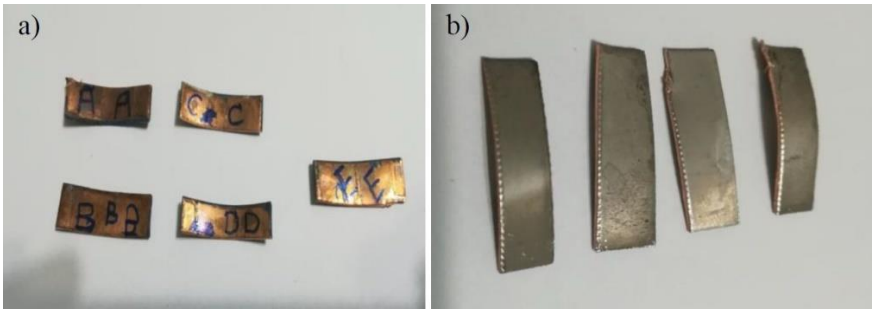

Figure 3. The coating specimens. a) The copper substrate and b) The coated surface.

In the electrochemical corrosion test, specifically the potentiodynamic polarization test, the specimen is polarized relative to its equilibrium condition. In other words, the sample potential is varied positively or negatively from the equilibrium potential or Open Circuit Potential (OCP). The OCP is the potential difference between the working electrode and the reference electrode when the sample is exposed to the electrolyte in an equilibrium state, with no measurable corrosion current. The OCP should stabilize at a constant potential with minimal fluctuations. The surface area of the sample must be accurately determined for current density calculations.

Each corrosion test involves three electrodes: a working electrode, a counter electrode, and a reference electrode, chosen according to the coating type and corrosion environment. In this research, a saturated Calomel reference electrode was used. To obtain the cathodic and anodic branch slopes, two appropriate points were selected on each branch, and the intersection of these slopes was calculated to determine the corrosion current density. The Tafel and potentiodynamic test parameters were extracted using Nova 2.1.4 software. The corrosion current density is calculated using the

following equation:

$$i_{corr} = \frac{\beta_a \beta_c}{2.303(\beta_a+\beta_c)R_p} \quad (4)$$

where β_a describes the anodic branch slope, β_c represents the cathodic branch slope, and R_p points out the polarization resistance, which is defined as the potential difference variations versus the current alterations [3]. Through the determination of corrosion current density, the corrosion rate can be obtained via the below relation:

$$CR^1\left(\frac{mm}{y}\right) = 3.27 \times i_{corr}\left(\frac{mA}{cm^2}\right) \times \frac{Ew}{D} \quad (5)$$

where EW stands for equivalent weight and D indicates density, both of which are equal to 63.5 g/mol and 8.96 g/cm^3 for nickel, respectively.

Electrochemical impedance spectroscopy (EIS) was performed after the electrodeposition process using a three-electrode cell containing a 3.5 wt.% NaCl solution. A calomel electrode was used as the reference electrode, and a counter electrode was also included. Prior to each experiment, the specimens were immersed in the corrosion cell and exposed to the electrolyte to monitor the Open Circuit Potential (OCP) for a specific period (e.g., 15 minutes) until the potential stabilized. The EIS analysis was then conducted over a frequency range from 100,000 Hz to 0.01 Hz, with a sinusoidal AC potential applied at an amplitude of ±10 mV versus OCP for all pure nickel and Ni-B_4C nanocomposite coating samples. The extracted EIS parameters were subsequently fitted using ZViewTM software (Version 3.4, Scribner Associates Inc.).

2-5 – MORPHOLOGICAL STUDIES VIA FESEM

To identify the morphology of the pure nickel and nickel-B_4C nanocomposite coating samples, FESEM analysis was performed using a MIRA3 TESCAN model instrument. Prior to the microstructural assessment and evaluation of electrical conductivity, the specimen surfaces were coated with a very thin layer of gold.

2-6 – CHEMICAL CHARACTERIZATION VIA EDS

EDS (or EDX) and MAP analysis were performed on the coating samples for chemical characterization. EDX analysis was used to determine the incorporation rate of B_4C nanoparticles in the nanocomposite coating. The weight percentages (wt.%) of Ni, B, and C in the coating matrix were calculated using EDX analysis and subsequently converted to volume percentages (vol.%). The volume percentages (vol.%) were derived using the following equations:

$$\text{The wt.\% of } B_4C = \frac{\text{Boron (B) \% obtained from EDAX} \times B_4C \text{ molar mass}}{\text{Boron molar mass}} \quad (6)$$

$$\text{The wt.\% of Ni} = 100 - \text{The wt.\% of } B_4C \quad (7)$$

where B_4C molar mass is 55.255 g/mol, B molar mass is 10.811 g/mol, and C molar mass is 12.011 g/mol. The B_4C incorporation rate (vol. %) is then calculated via Equation 8:

$$B_4C \text{ vol.\%} = \frac{100 \times \frac{\text{The wt.\% of } B_4C}{B_4C \text{ density}}}{\frac{\text{The wt.\% of Ni}}{\text{Nickel density}} + \frac{\text{The wt.\% of } B_4C}{B_4C \text{ density}}} \quad (8)$$

where B_4C density is 2.52 g/cm^3, Nickel density is 8.9 g/cm^3, and Carbon density is 2.2 g/cm^3.

2-7 – MICROSTRUCTURAL ASSESSMENT BY XRD STUDIES

To investigate the crystalline microstructure of the pure Ni and Ni-B_4C coatings, X-ray diffraction (XRD) analysis was conducted using a Philips Bruker D8 diffractometer with a copper Kα source. The reported findings were analyzed using Xpert High Score Plus software.

3- RESULTS AND DISCUSSION

3-1 – CHEMICAL COMPOSITION AND MORPHOLOGY OF Ni-B4C

The microstructure and morphology of pure nickel and nickel nanocomposite coatings reinforced with B_4C nanoparticles were evaluated using FESEM, EDS, and MAP analysis. These analyses investigated the incorporation of B_4C nanoparticles and the effects of pulse electrodeposition (PE) parameters on the microstructure of the coatings. Table 5 categorizes the specimens based on their PE parameters. The baseline sample, E, represents pure nickel, while samples A to D denote Ni-B_4C pulse electrodeposited nanocomposite coatings.

Table 5. Vol. % of B_4C nanoparticles regarding the pulse electrodeposition parameters

Sample	i (A/dm^2)	f (Hz)	γ (%)	Vol. % B_4C
A (Baseline Ni-B_4C)	1	10	50	5.5
B (Ni-B_4C)	4	10	50	2.9
C (Ni-B_4C)	1	10	25	4.6
D (Ni-B_4C)	1	1	50	3.9
E (Baseline Ni)	1	10	50	0

Figure 4a and 4b show the BSE and EDS analyses of the baseline Ni-B_4C nanocomposite coating deposited under conditions of i_{corr} = 1 A/dm^2, γ = 50 %, f = 10 Hz. The map analysis of Boron and Carbon distribution confirms the incorporation of these elements into the nickel coating matrix.

[1] Corrosion Rate (CR)

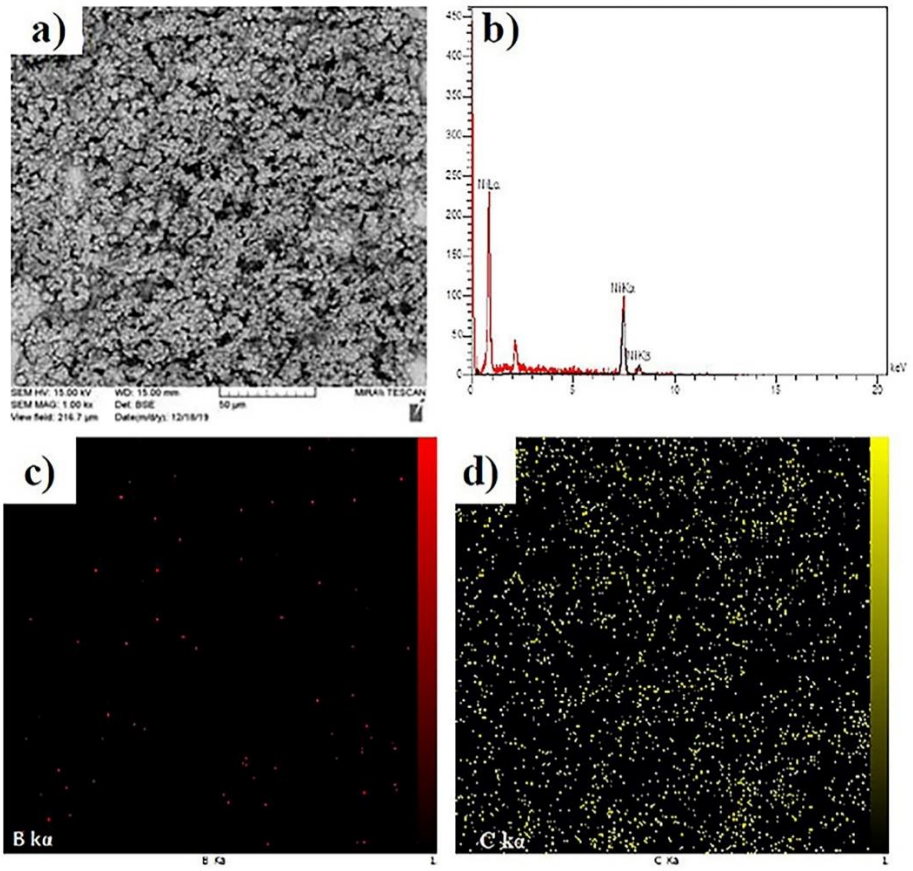

Figure 4. BSE and EDS analysis of the Ni-B_4C baseline nanocomposite coating deposited under i_{corr} = 1 A/dm^2, f = 10 Hz, γ = 50 %. a) BSE micrograph at 50µm, b) EDS spectrum, c) Boron distribution map, and d) Carbon distribution map.

The FESEM micrographs of pure nickel and Ni-B_4C nanocomposite coatings fabricated under the baseline electrodeposition conditions are shown in Figure 5a and 5b. Figure 5a demonstrates the morphology of pure Ni, which consists of fine nickel pyramids. In contrast, the incorporation of 5.5 vol.% B_4C nanoparticles into the nickel matrix transformed the coating morphology from nickel pyramids (see Figure 5a) to a spherical (nodular) microstructure (see Figure 5b). Similar microstructures have also been observed in other studies on composite coatings, such as Ni-Mo [62], Ni-Cr [63], Ni-WC [64], Ni-ZnO [31], and Ni- Si_3N_4 [33].

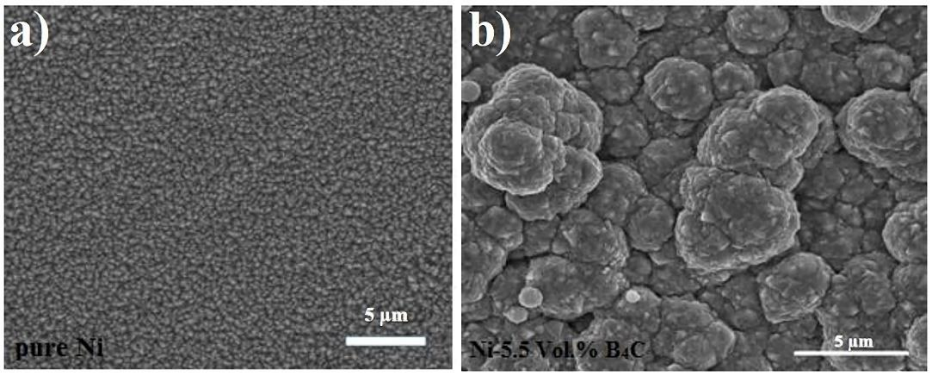

Figure 5. The FESEM micrographs of baseline pure nickel and Ni-B_4C nanocomposite coatings

The FESEM micrographs of Ni-B_4C nanocomposite coatings produced at 1 and 4 A/dm^2, under baseline conditions (f = 10 Hz, γ = 50 %.) are demonstrated in Figure 6. a and b.

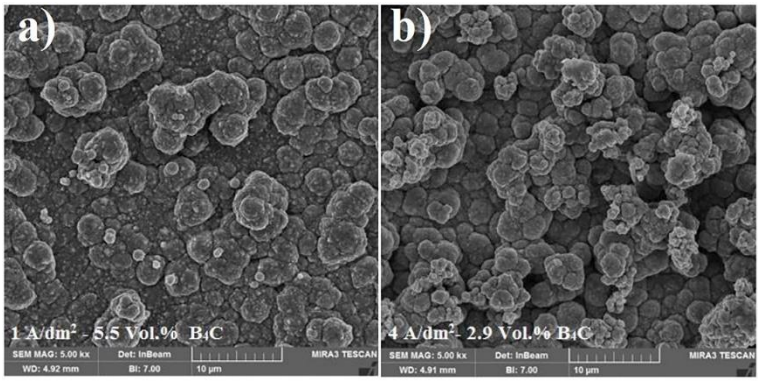

Figure 6. The FESEM micrographs of Ni-B_4C nanocomposite coatings deposited under f = 10 Hz, γ = 50 %. at: a) 1 A/dm^2 and b) 4 A/dm^2

As depicted in Figure 6, increasing the current density from 1 to 4 A/dm² resulted in changes in the microstructure and a decrease in the incorporation rate of B_4C nanoparticles, from 5.5 to 2.9 vol.%. This indicates that, despite the higher driving force, the reduction rate of deposited nanoparticles was diminished. The reduction rate of Ni^{2+} ions exceeded the adsorption rate of nanoparticles on the surface, leading to a decrease in B_4C nanoparticle incorporation [65]. In other words, while increasing the pulse current density initially leads to more deposition of B_4C nanoparticles in the coating, at higher current densities, the diffusion of Ni atoms into the matrix surpasses that of the B_4C nanoparticles, resulting in a significant reduction in B_4C incorporation. Dini et al. [66] noted that increasing the pulse current density to a certain limit raises the overpotential and increases the nucleation rate, ultimately resulting in a microstructure with finer grains. by Ebrahimi et al. [67] explained that the enhancement of electroplating current density leads to a reduction in nickel ion reduction in the microstructure and co-deposition of hydrogen at the cathode-electrolyte interface. Rashidi and Amadeh [68] also found that increasing the electroplating current density from 1 to 5 A/dm² reduced the grain size, although further increases in current density led to a nearly constant grain size.

As observed in Figure 7, increasing the duty cycle from 25% to 50% led to a higher incorporation rate of B_4C nanoparticles, from 4.6 to 5.5 vol.%. This increase can be attributed to the relationship $i_m = i_p \times \gamma$ (refer to relation 3 in the Introduction), where the average current density rises with the duty cycle, resulting in a greater amount of nanoparticles incorporated into the coating [16]. Specifically, at lower duty cycles (short TON or long TOFF), the coating tends to have high impact but may exhibit negligible porosity. In such cases, the nanoparticles embedded in the coating may have weak connections, making the coating prone to separation or peeling. Increasing the duty cycle enhances the incorporation rate of nanoparticles into the coating. However, when the duty cycle is further increased to 75%, the nanoparticle incorporation rate decreases. This is associated with a rise in current density and a significant increase in grain size [16, 50].

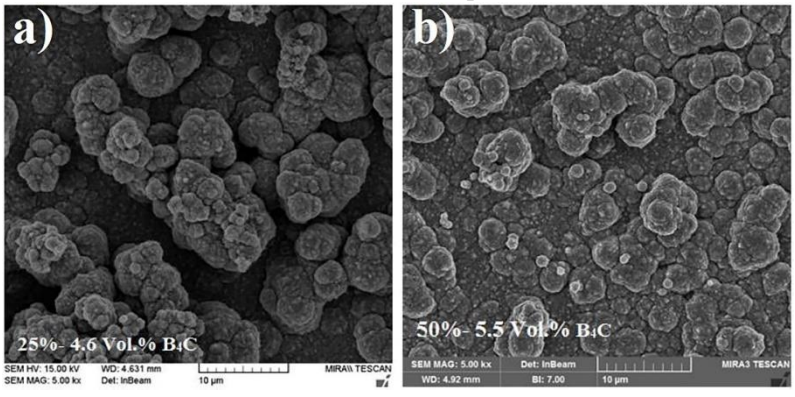

Figure 7. The FESEM micrographs of Ni-B_4C nanocomposite coatings deposited under i_{corr} = 1 A/dm^2, f = 10 Hz, at duty cycle of a) γ = 25 % and b) γ = 50 %

Figure 8 illustrates the changes in morphology as the pulse frequency increased from 1 to 10 Hz. Raising the pulse frequency from 1 to 10 Hz for the Ni-B_4C samples resulted in an increase in B_4C nanoparticle incorporation from 3.9 to 5.5 vol.%. This improvement is due to the reduction in total electrodeposition time (T_{ON}+ T_{OFF}) and the increased number of electrodeposition cycles, which leads to a higher percentage of nanoparticles being incorporated into the coating [14]. Chen et al. [69] demonstrated that increasing the pulse frequency, which results in a higher number of deposition cycles and shorter T_{ON} and T_{OFF} periods, enhances the incorporation of the secondary reinforcing phase into the matrix.

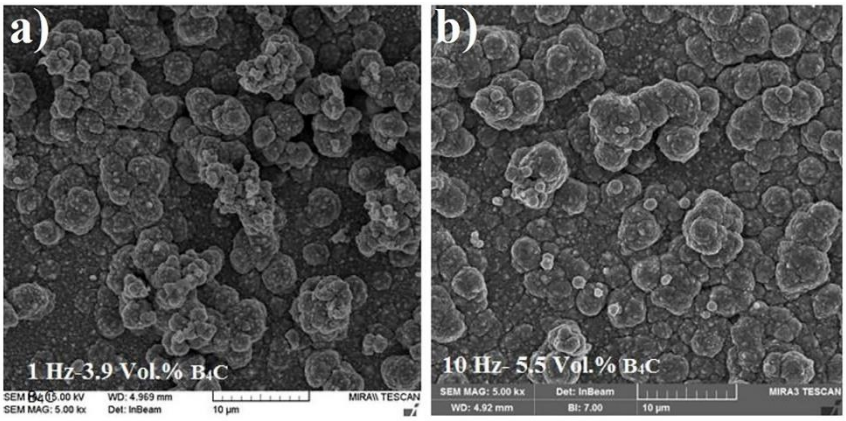

Figure 8. The FESEM micrographs of Ni-B_4C nanocomposite coatings deposited under i_{corr} = 1 A/dm^2, γ = 50 % at pulse frequencies of a) f = 1 Hz and b) f = 10 Hz

Sajjadnejad et al. [3] found that increasing the pulse current density led to a significant increase in the number of nanoparticles deposited in Ni-nanodiamond composite coatings. Similar results were reported by Lajevardi and Sharabi [70] for Ni-TiO_2 composite coatings. Additionally, our recent study on the wear and tribological properties of Ni-B_4C nanocomposite coatings showed a substantial improvement in microhardness across all Ni-B_4C specimens deposited under different electrodeposition parameters, compared to pure nickel coatings [71].

3-2- MICROSTRUCTURAL STUDIES VIA XRD ANALYSIS FINDINGS

In this section, the XRD results of pure nickel and nickel-B_4C nanocomposite coatings were determined and the effect of B_4C incorporation on the microstructure and the crystallite size of the coatings is thoroughly investigated.

The embedment of B_4C nanoparticles in the nickel matrix led to an increase in the peak broadening in XRD spectrum peaks so that the crystallite size experienced a huge reduction in the Ni- B_4C coating compared to pure Ni coating. The crystallite size of the main peaks was obtained via Scherrer's equation and the obtained results are given in Table 6. To assess the influence of B_4C nanoparticles on the coating characteristics, the size of crystallites was determined by Xpert software using Scherrer's equation as follows:

$$d = \frac{K\lambda}{\beta Cos\theta} \quad (9)$$

where D indicates the size of crystallites, k denotes the shape factor constant approximately taken as 1 for particles or crystallites and 0.94 precisely for spherical crystallites, λ describes the X-ray wavelength in nm, β represents the peak width at the half intensity or FWHM (Full Width Half Maximum) shown in radians, and θ is the diffraction angle in radians [72]. The peak broadening is initiated by crystal defects, twin boundaries, strain, and crystallite size.

Table 6- The XRD analysis results for pure Ni and Ni-B_4C nanocomposite baseline samples obtained via the Scherrer technique.

Sample	2θ (°)	(hkl)	FWHM	d (nm)
Pure Ni	44.239	(111)	0.12	73.2
	50.431	(200)	0.192	44.7
Ni-B_4C	44.898	(111)	-	32
	52.148	(200)	-	23

Figure 9 and Table 6 show the XRD spectrum for both pure Ni and Ni-B_4C coatings. The data reveal that incorporating B_4C nanoparticles into the matrix significantly reduced the relative intensity of the (111) and (200) crystal planes. Additionally, the crystallite size of nickel decreased notably for these planes, from 73.2 nm to 32 nm for (111) and from 44.7 nm to 23 nm for (200). The presence of B_4C nanoparticles increases the number of nucleation sites, which contributes to the reduction in crystallite size [3].

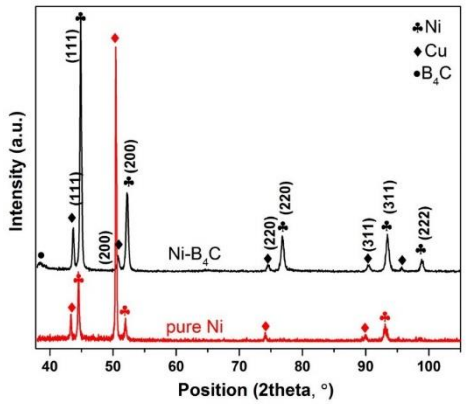

Figure 9. The XRD spectrum for pure nickel and Ni-B_4C nanocomposite coatings

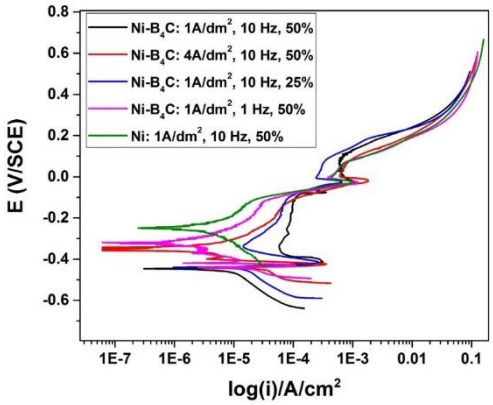

Figure 10. The potentiodynamic polarization curves for pure Ni and Ni-B_4C coatings under variant electrodeposition parameters

Li et al. [73] observed that the primary structure of nickel-diamond coatings at $2\theta = 43.2°$ is FCC, which aligns with our findings. As shown in Table 6, the inclusion of B_4C nanoparticles in the nickel coating contributes to a significant reduction in the crystallite size of the main peaks. This effect is primarily due to the B_4C nanoparticles acting as a reinforcing phase and creating additional nucleation sites within the nickel grain boundaries, resulting in a finer microstructure. Moreover, Tao et al. [74] proved nanoparticle incorporation as the main reason for peak broadening and decrease in the crystallite size of the Ni-B-Sc composite coating.

3-3 – THE CORROSION CHARACTERISTICS

The corrosion characteristics of pure nickel and nickel-B_4C nanocomposite coatings were evaluated using potentiodynamic polarization and electrochemical impedance spectroscopy (EIS).

Figure 10 shows the potentiodynamic polarization curves for both pure Ni and Ni-B_4C nanocomposite coatings. The curves reveal two distinct anodic and cathodic branches in the active region, as well as the passive and trans-passive regions beyond them.

Figure 10 illustrates the potentiodynamic polarization curve demonstrating the active-passive behavior typical of pure nickel coatings. This curve is divided into three critical regions: i. Active, ii. Passive, and iii. Transpassive. The pitting potential (E_{pit}) is the boundary between the passive region and the beginning of the transpassive region.

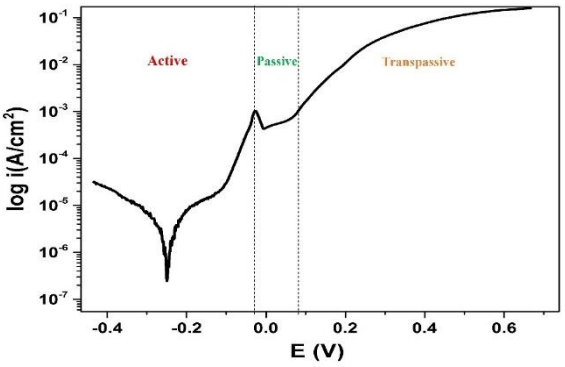

Figure 11. The typical potentiodynamic polarization curve for pure Ni coating with an active-passive corrosion behavior exhibiting active, passive, and trans-passive regions.

The extracted data from potentiodynamic polarization tests such as corrosion current density (i_{corr}), corrosion potential (E_{corr}), and pitting potential (E_{pit}) for all pure Ni and Ni-B_4C coatings under various pulse electrodeposition parameters are shown in Table 7.

Table 7- The extracted data from the potentiodynamic polarization test for all pure Ni and Ni-B_4C coatings under variant pulse electrodeposition parameters

Sample	Chemical composition of coating	B_4C concentration (g/L)	Current density (A/dm^2)	Duty cycle (%)	Pulse frequency (Hz)	B_4C Incorporation rate (vol. %)	Corrosion potential)V vs. SCE(	Corrosion current density ($\mu A/cm^2$)	Corrosion rate (mm/year)	Pitting potential (E_{pit}) – (V vs. SCE)
A	Ni-B_4C	5	1	50	10	5.5	-0.446	4.541	0.048	0.105
B	Ni-B_4C	5	4	50	10	2.9	-0.353	1.375	0.011	0.081
C	Ni-B_4C	5	1	25	10	4.6	-0.439	7.243	0.077	0.086
D	Ni-B_4C	5	1	50	1	3.9	-0.32	0.599	0.006	0.073
E	Ni	0	1	50	10	0	-0.249	2.301	0.024	0.055

Figure 10 and Table 7 show that the best corrosion resistance was observed in the D sample, a Ni-B_4C coating deposited under i = 1 A/dm², γ = 50 %, and f = 1 Hz, which had the lowest corrosion current density of 0.559 µA/cm². Interestingly, despite an incorporation rate of 5.5%, B_4C nanoparticles led to an increase in corrosion current density from 2.301 to 4.541 µA/cm² in the baseline condition (i = 1 A/dm², γ = 50 %, and f = 10 Hz). This increase is likely due to uneven distribution and participation of B_4C nanoparticles in the nickel matrix. Nonetheless, the Ni-B_4C nanocomposite coatings, specifically samples B (deposited under i = 4 A/dm², γ = 50 %, and f = 10 Hz) and D (deposited under i = 1 A/dm², γ = 50 %, and f = 1 Hz), demonstrated lower corrosion current densities and thus better corrosion resistance compared to pure nickel coatings.

Increasing the pulse current density from 1 to 4 A/dm² led to a significant reduction in corrosion current density from 4.541 to 1.375 µA/cm², while the B_4C incorporation rate decreased from 5.5 to 2.9 vol.%. This improvement is likely due to a more uniform distribution and greater compaction of the nanocomposite coating achieved at 4 A/dm². Amadeh et al. [75] observed similar trends in their study on Ni-SiC coatings, where raising the pulse current density from 2 to 8 A/dm² reduced corrosion current density significantly, although the corrosion potential shifted to a more negative value and no major changes were noted in the passive region. Sajjadnejad et al. [16] found that for Ni-diamond coatings, increasing the pulse current density from 1 to 4 A/dm² resulted in a more positive corrosion potential and lower corrosion current density. However, further increasing the current density to 10 A/dm² reduced corrosion resistance, attributed to higher participation at 4 A/dm² and reduced B_4C incorporation at higher current densities.

Increasing the duty cycle from 25% to 50% in Ni-B_4C coatings resulted in a reduction in corrosion current density from 7.243 to 4.541 µA/cm², which was associated with an increase in B_4C nanoparticle incorporation from 4.6% to 5.5% vol.%. Sajjadnejad et al. [16] observed a similar trend, noting that while increasing the duty cycle improved B_4C incorporation up to a certain point, further increases in the duty cycle led to a reduction in nanoparticle incorporation.

On the other hand, increasing the pulse frequency from 1 to 10 Hz caused a notable rise in corrosion current density from 0.599 to 4.541 µA/cm². This decline in corrosion resistance was linked to a higher B_4C incorporation rate, from 3.9% to 5.5% vol.%, which suggests that the more uniform distribution of B_4C nanoparticles at lower frequencies contributed to this effect. Shahrabi et al. [70] found similar results with Ni-TiO_2 coatings, where increasing pulse frequency improved corrosion resistance. In contrast, Sajjednejad et al. [3] observed that higher pulse frequencies led to increased overpotential and altered surface topography, which enhanced B_4C nanoparticle incorporation and improved corrosion resistance. Amadeh et al. [75] reported that raising the pulse frequency from 10 to 1000 Hz decreased corrosion current density due to increased B_4C nanoparticle incorporation in Ni-SiC coatings. Medelien et al. [76] noted that B_4C incorporation shifted the corrosion potential to more negative values and increased the electrochemical activity of the nickel coating, attributing reduced corrosion resistance to the semi-conductive behavior of B_4C. Jiang et al. found that increasing B_4C concentration from 2 to 8 g/L shifted the Tafel curves to positive potentials and enhanced corrosion resistance, which was ascribed to the uniform and compact structure of the Ni-B_4C nanocomposite coatings [77].

As seen in Table 7 and Figure 10, the incorporation of B_4C nanoparticles into the nickel matrix caused a significant positive shift in the pitting potential E_{pit} for all Ni-B_4C coatings compared to the pure nickel coating. This shift can be attributed to the inhibitory effect of B_4C particles, which help to fill surface defects and porosities, thereby preventing the diffusion of highly corrosive ions, particularly chloride ions (Cl^-), present in the NaCl corrosive environment studied in this research. Furthermore, the B_4C incorporation extended the passive region for all Ni-B_4C coatings relative to the pure nickel coating, indicating enhanced corrosion resistance.

The EIS curves including the Nyquist, Bode-magnitude, and Bode-phase plots for pure Ni and Ni-B_4C nanocomposite coating deposited under i = 1 A/dm², γ = 50 %, f = 10 Hz and i = 1 A/dm², γ = 50 %, and f = 1 Hz, respectively, are presented in Figure 12.

To achieve optimal EIS curve fitting for the pure Ni and Ni-B_4C coatings, the recommended equivalent circuit is displayed in Figure 13. The fitting was performed using ZView™ software based on the data extracted from EIS analysis. In this circuit, **Rs** represents the solution resistance, **Rct** denotes the charge transfer resistance, and **CPE_{dl}** refers to the constant phase element of the double-layer. The presence of a single capacitance loop or semicircular arc in the Nyquist plot indicates a charge transfer corrosion mechanism, while the Bode plots for both pure Ni and Ni-B_4C coatings show only one time constant. This equivalent circuit and its fitting curve were thus used for data analysis and discussion. Similar equivalent circuits were applied by Li et al. [59] and Omidvar et al. [78] for assessing the corrosion characteristics of the Ni-W-B_4C coatings and NiBP-graphite coatings, respectively.

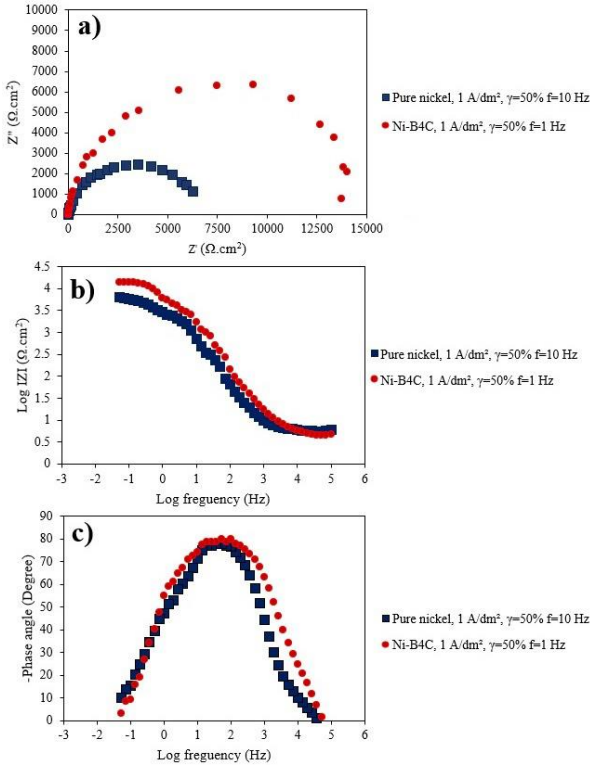

Figure 12. The Nyquist, Bode magnitude, and Bode phase plots extracted from the EIS obtained results for pure nickel deposited under i = 1 A/dm^2, γ = 50 %, f = 10 Hz and nickel-B_4C nanocomposite coating fabricated at i = 1 A/dm^2, γ = 50 %, f = 1 Hz

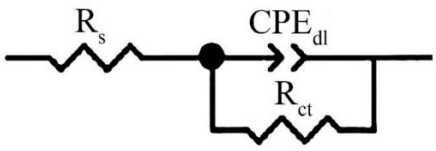

Figure 13. The equivalent circuit for fitting the EIS curves of pure Ni and Ni-B_4C coating

The values obtained by fitting the EIS curves are reported in Table 8. The table compares the pure nickel coating with the Ni-B_4C coating specimen, which exhibits the lowest corrosion current density (as presented in Table 7). The coatings were deposited under the conditions of **i = 1 A/dm², γ = 50%, f = 10 Hz** for the baseline, and **i = 1 A/dm², γ = 50%, f = 1 Hz** for the sample with minimum corrosion current density. This comparison highlights the enhanced corrosion resistance observed in the Ni-B_4C nanocomposite coating due to the optimized electrodeposition parameters.

Table 8. The electrochemical parameters obtained from the EIS analysis via the fitting curve.

Sample	R_s (Ω.cm^2)	R_{ct} (Ω.cm^2)	CPE_{dl} or Y_0 (s^n.cm^{-2}.Ω^{-1})	n
Pure Nickel (*i* = 1 A/dm^2, γ = 50 %, f = 10 Hz)	5.752	5504	3.18 × 10^{-5}	0.943
Ni-B_4C (*i* = 1 A/dm^2, γ = 50 %, f = 1 Hz)	4.744	13517	1.47 × 10^{-5}	0.935

According to Table 8, incorporating B_4C into the nickel matrix, along with lowering the pulse frequency, led to a significant increase in the charge transfer resistance (**Rct**) from 5504 Ω.cm² for pure nickel to 13515 Ω.cm² for the Ni-B_4C coating. This rise in **Rct** indicates a notable improvement in corrosion resistance, aligning with the results of corrosion current density and corrosion rate (as seen in Table 7). The reduction in the double-layer constant phase element (**CPE_{dl}**) further supports this enhancement in **Rct** and overall corrosion resistance. The **n** value, which remained close to 1, signifies near-ideal electrochemical behavior (refer to Figure 12 and Table 8).

CONCLUSION

In this study, pure nickel and Ni-B_4C nanocomposite coatings were synthesized using the pulse electrodeposition (PE) technique. The effects of B_4C nanoparticle incorporation and pulse parameters—such as pulse current density, duty cycle, and pulse frequency—on the coatings' microstructure, morphology, and nanoparticle distribution were analyzed through EDS, FESEM, and XRD methods. The corrosion behavior of the coatings was also assessed via potentiodynamic polarization and electrochemical impedance spectroscopy (EIS). Key findings include:

1) Electrodeposition was conducted with a baseline of **i = 1 A/dm², γ = 50%, f = 10 Hz**.
2) The addition of B_4C nanoparticles changed the nickel coating's morphology from a pyramid-like structure to a spherical (nodular) form.
3) Increasing the pulse current density from **1 to 4 A/dm²** reduced the incorporation of B_4C from **5.5 to 2.9 vol.%**, while increasing the duty cycle from **25% to 50%** and pulse frequency from **1 to 10 Hz** boosted B_4C incorporation from **4.6 vol.%** and **3.9 vol.%** to **5.5 vol.%**, respectively.
4) The incorporation of B_4C nanoparticles reduced the crystallite size of nickel for the **(111)** and **(200)** crystal planes from **73.2 to 32 nm** and **44.7 to 23 nm**, respectively.

5) The incorporation of B_4C nanoparticles increased the corrosion current density from **2.301 to 4.541 µA/cm²** under baseline conditions.
6) The lowest corrosion current density of **0.559 µA/cm²** (indicating the best corrosion resistance) was observed in the Ni-B_4C coating deposited under **i = 1 A/dm², γ = 50%, f = 1 Hz**. Increasing the pulse current density from **1 to 4 A/dm²** and the duty cycle from **25% to 50%** significantly reduced the corrosion current density from **4.541 to 1.375 µA/cm²** and from **7.243 to 4.541 µA/cm²**, respectively. Conversely, raising the pulse frequency from **1 to 10 Hz** increased the corrosion current density from **0.599 to 4.541 µA/cm²**, despite a rise in B_4C incorporation from **3.9 to 5.5 vol.%** due to a more uniform nanoparticle distribution at **1 Hz**.
7) The Ni-B_4C coating deposited at **1 Hz** demonstrated a higher **Rct** compared to the pure nickel coating, aligning with both EIS and potentiodynamic polarization results.

REFERENCES

1. Raghavendra, C. R., Basavarajappa, S., & Sogalad, I. (2018). Electrodeposition of Ni-nano composite coatings: a review. *Inorganic and Nano-Metal Chemistry*, *48*(12), 583-598. https://doi.org/10.1080/24701556.2019.1567537
2. Mahidashti, Z., Aliofkhazraei, M., & Lotfi, N. (2018). Review of nickel-based electrodeposited tribo-coatings. *Transactions of the Indian Institute of Metals*, *71*, 257-295. https://doi.org/10.1007/s12666-017-1175-x
3. Sajjadnejad, M., Omidvar, H., Javanbakht, M., & Mozafari, A. (2017). Textural and structural evolution of pulse electrodeposited Ni/diamond nanocomposite coatings. *Journal of Alloys and Compounds*, *704*, 809-817. https://doi.org/10.1016/j.jallcom.2016.12.318
4. Sajjadnejad, M., Haghshenas, S.M.S., Mehr Monjezi, M. (2022).Assessment of Failure Mechanisms in an Industrial Firewater Pipeline: A Case Study. *Advanced Journal of Chemistry-Section A, 5(2)*, 81-93. https://doi.org/10.22034/ajca.2022.324623.1298
5. Sahab, A. R. M., Saad, N. H., Kasolang, S., & Saedon, J. (2012). Impact of plasma spray variables parameters on mechanical and wear behaviour of plasma sprayed Al2O3 3% wt TiO2 coating in abrasion and erosion application. *Procedia Engineering*, *41*, 1689-1695. https://doi.org/10.1016/j.proeng.2012.07.369
6. Luo, L., Yao, J., Li, J., & Yu, J. (2009). Preparation and characterization of sol–gel Al2O3/Ni–P composite coatings on carbon steel. *Ceramics International*, *35*(7), 2741-2745. https://doi.org/10.1016/j.ceramint.2009.03.019
7. Ba, K., Chahine, A., Ebn Touhami, M., Alauzun, J. G., & Manseri, A. (2020). Preparation and characterization of phosphate-nickel-titanium composite coatings obtained by sol–gel process for corrosion protection. *SN Applied Sciences*, *2*, 1-13. https://doi.org/10.1007/s42452-020-2173-x
8. Sajjadnejad, M., & Karimi Abadeh, H. (2019). Kinetics of photocatalytic degradation of methylene blue on nanostructured TiO2 coatings created by sol-gel process. *Advanced Ceramics Progress*, *5*(1), 1-8. https://doi.org/10.30501/acp.2019.93123
9. Bolelli, G., Berger, L. M., Bonetti, M., & Lusvarghi, L. (2014). Comparative study of the dry sliding wear behaviour of HVOF-sprayed WC–(W, Cr) 2C–Ni and WC–CoCr hardmetal coatings. *Wear*, *309*(1-2), 96-111. https://doi.org/10.1016/j.wear.2013.11.001
10. Bose, K., Wood, R. J. K., & Wheeler, D. W. (2005). High energy solid particle erosion mechanisms of superhard CVD coatings. *Wear*, *259*(1-6), 135-144. https://doi.org/10.1016/j.wear.2005.02.043
11. Grzesik, W., Zalisz, Z., Krol, S., & Nieslony, P. (2006). Investigations on friction and wear mechanisms of the PVD-TiAlN coated carbide in dry sliding against steels and cast iron. *Wear*, *261*(11-12), 1191-1200. https://doi.org/10.1016/j.wear.2006.03.004
12. Karmakar, R., Maji, P., & Ghosh, S. K. (2021). A review on the nickel based metal matrix composite coating. *Metals and Materials International*, *27*, 2134-2145. https://doi.org/10.1007/s12540-020-00872-w
13. Low, C. T. J., Bello, J. O., Wharton, J. A., Wood, R. J. K., Stokes, K. R., & Walsh, F. C. (2010). Electrodeposition and tribological characterisation of nickel nanocomposite coatings reinforced with nanotubular titanates. *Surface and Coatings Technology*, *205*(7), 1856-1863. https://doi.org/10.1016/j.surfcoat.2010.08.054
14. Sajjadnejad, M., Mozafari, A., Omidvar, H., & Javanbakht, M. (2014). Preparation and corrosion resistance of pulse electrodeposited Zn and Zn–SiC nanocomposite coatings. *Applied Surface Science*, *300*, 1-7. https://doi.org/10.1016/j.apsusc.2013.12.143
15. Sajjadnejad, M., Omidvar, H., & Javanbakht, M. (2017). Influence of pulse operational parameters on pure nickel electrodeposits: Part II. Microhardness and corrosion resistance. *Surface Engineering*, *33*(2), 94-101. https://doi.org/10.1080/02670844.2015.1122140
16. Sajjadnejad, M., Omidvar, H., & Javanbakht, M. (2017). Influence of pulse operational parameters on electrodeposition, morphology and microstructure of Ni/nanodiamond composite coatings. *International Journal of Electrochemical Science*, *12*(5), 3635-3651. https://doi.org/10.20964/2017.05.52
17. Sajjadnejad, M., Setoudeh, N., Mozafari, A., Isazadeh, A., & Omidvar, H. (2017). Alkaline electrodeposition of Ni–ZnO nanocomposite coatings: effects of pulse electroplating parameters. *Transactions of the Indian Institute of Metals*, *70*, 1533-1541. https://doi.org/10.1007/s12666-016-0950-4
18. Rajak, D. K., Wagh, P. H., Menezes, P. L., Chaudhary, A., & Kumar, R. (2020). Critical overview of coatings technology for metal matrix composites. *Journal of Bio-and Tribo-Corrosion*, *6*, 1-18. https://doi.org/10.1007/s40735-019-0305-x
19. Gül, H., Uysal, M., Akbulut, H., & Alp, A. (2014). Effect of PC electrodeposition on the structure and tribological behavior of Ni–Al2O3 nanocomposite coatings. *Surface and Coatings Technology*, *258*, 1202-1211. https://doi.org/10.1016/j.surfcoat.2014.07.002
20. Wang, L., Gao, Y., Xu, T., & Xue, Q. (2006). Corrosion resistance and lubricated sliding wear behaviour of novel Ni–P graded alloys as an alternative to hard Cr deposits. Applied Surface Science, 252(20), 7361-7372. https://doi.org/10.1016/j.apsusc.2005.08.040
21. Mehr, M. S., Akbari, A., & Damerchi, E. (2019). Electrodeposited Ni-B/SiC micro-and nano-composite coatings: a comparative study. Journal of Alloys and Compounds, 782, 477-487. https://doi.org/10.1016/j.jallcom.2018.12.184
22. Ma, C., He, H., Xia, F., Xiao, Z., & Liu, Y. (2023). Performance of Ni–SiC composites deposited using magnetic-field-assisted electrodeposition under different magnetic-field directions. Ceramics International, 49(22), 35907-35916. https://doi.org/10.1016/j.ceramint.2023.08.271
23. Paydar, S., Jafari, A., Bahrololoom, M. E., & Mozafari, V. (2015). Influence of BN and B4C particulates on wear and corrosion resistance of electroplated nickel matrix composite coatings. Tribology-Materials, Surfaces & Interfaces, 9(2), 105-110. https://doi.org/10.1179/1751584X15Y.0000000007
24. Zhang, Y., Zhang, S., He, Y., Li, H., He, T., Fan, Y., & Zhang, H. (2021). Mechanical properties and corrosion resistance of pulse electrodeposited Ni-B/B4C composite coatings. Surface and Coatings Technology, 421, 127458. https://doi.org/10.1016/j.surfcoat.2021.127458
25. Torkamani, A. D., Velashjerdi, M., Abbas, A., Bolourchi, M., & Maji, P. (2021). Electrodeposition of Nickel matrix composite coatings via various Boride particles: A review. Journal of Composites and Compounds, 3(7), 106-113. https://doi.org/10.52547/jcc.3.2.4

26. Mohajeri, S., Dolati, A., & Rezagholibeiki, S. (2011). Electrodeposition of Ni/WC nano composite in sulfate solution. Materials Chemistry and Physics, 129(3), 746-750. https://doi.org/10.1016/j.matchemphys.2011.04.053
27. Algul, H., Gul, H., Uysal, M., Alp, A., & Akbulut, H. (2015). Tribological properties of TiO 2 reinforced nickel based MMCs produced by pulse electrodeposition technique. *Transactions of the Indian Institute of Metals*, *68*, 79-87. https://doi.org/10.1007/s12666-014-0444-1
28. [28] Sajjadnejad, M., Karkon, S., & Haghshenas, S. M. S. (2024). Corrosion Characteristics of Zn-TiO_2 Nanocomposite Coatings Fabricated by Electro-Codeposition Process. *Advanced Journal of Chemistry, Section A*, *7*(2), 209-226. https://doi.org/10.48309/ajca.2024.418391.1425
29. Bahrololoom, M. E., & Sani, R. (2005). The influence of pulse plating parameters on the hardness and wear resistance of nickel–alumina composite coatings. Surface and Coatings Technology, 192(2-3), 154-163. https://doi.org/10.1016/j.surfcoat.2004.09.023
30. Refai, M., Hamid, Z. A., El-kilani, R. M., & Nasr, G. E. (2021). Electrodeposition of Ni–ZnO nano-composite for protecting the agricultural mower steel knives. Chemical Papers, 75, 139-152. https://doi.org/10.1007/s11696-020-01291-2
31. Sajjadnejad, M., Haghshenas, S. M. S., Targhi, V. T., Setoudeh, N., Hadipour, A., Moghanian, A., & Hosseinpour, S. (2021). Wear behavior of alkaline pulsed electrodeposited nickel composite coatings reinforced by ZnO nanoparticles. Wear, 468, 203591. https://doi.org/10.1016/j.wear.2020.203591
32. [32] Mirzamohammadi, S., Aliov, M. K., Sabur, A. R., & Hassanzadeh-Tabrizi, A. (2010). Study of wear resistance and nanostructure of tertiary Al 2 O 3/Y 2 O 3/CNT pulsed electrodeposited ni-based nanocomposite. Materials Science, 46, 76-86. https://doi.org/10.1007/s11003-010-9266-4
33. [33] Sajjadnejad, M., Abadeh, H. K., Omidvar, H., & Hosseinpour, S. (2020). Assessment of Tribological behavior of nickel-nano Si3N4 composite coatings fabricated by pulsed electroplating process. *Surface Topography: Metrology and Properties*, *8*(2), 025009. https://doi.org/10.1088/2051-672X/ab7ae5
34. Xia, F., Li, C., Ma, C., Li, Q., & Xing, H. (2021). Effect of pulse current density on microstructure and wear property of Ni-TiN nanocoatings deposited via pulse electrodeposition. Applied Surface Science, 538, 148139. https://doi.org/10.1016/j.apsusc.2020.148139
35. Xia, F., Yan, P., Ma, C., Wang, B., & Liu, Y. (2023). Effect of different heat-treated temperatures upon structural and abrasive performance of Ni-TiN composite nanocoatings. Journal of Materials Research and Technology, 27, 2874-2881. https://doi.org/10.1016/j.jmrt.2023.10.173
36. Algul, H., Tokur, M., Ozcan, S., Uysal, M., Çetinkaya, T., Akbulut, H., & Alp, A. (2015). The effect of graphene content and sliding speed on the wear mechanism of nickel–graphene nanocomposites. Applied Surface Science, 359, 340-348. https://doi.org/10.1016/j.apsusc.2015.10.139
37. [37] Mirzamohammadi, S., Khorsand, H., & Aliofkhazraei, M. (2017). Effect of different organic solvents on electrodeposition and wear behavior of Ni-alumina nanocomposite coatings. Surface and Coatings Technology, 313, 202-213. https://doi.org/10.1016/j.surfcoat.2017.01.025
38. Noorbakhsh Nezhad, A. H., Rahimi, E., Arefinia, R., Davoodi, A., & Hosseinpour, S. (2020). Effect of substrate grain size on structural and corrosion properties of electrodeposited nickel layer protected with self-assembled film of stearic acid. Materials, 13(9), 2052. https://doi.org/10.3390/ma13092052
39. Omidvar, H., Sajjadnejad, M., Stremsdoerfer, G., Meas, Y., & Mozafari, A. (2016). Composite NiB–graphite and NiB–PTFE surface coatings deposited by the dynamic chemical plating technique. Materials and Manufacturing Processes, 31(1), 24-30. https://doi.org/10.1080/10426914.2015.1004691
40. Saghafi, M., Mahboubi, F., Mohajerzadeh, S., & Holze, R. (2015). Preparation of Co-Ni oxide/vertically aligned carbon nanotube and their electrochemical performance in supercapacitors. Materials and Manufacturing Processes, 30(1), 70-78. https://doi.org/10.1080/10426914.2014.952026
41. Sajjadnejad, M., Omidvar, H., Javanbakht, M., & Mozafari, A. (2015). Characterization of pure nickel coatings fabricated under pulse current conditions. International Journal of Materials and Metallurgical Engineering, 9(8), 1061-1065. https://doi.org/10.5281/zenodo.1109912
42. Chawla, K. K., & Chawla, K. K. (1998). Metal matrix composites (pp. 164-211). Springer New York. https://doi.org/10.1007/978-1-4757-2966-5_6
43. Imanian Ghazanlou, S., Farhood, A. H. S., Ahmadiyeh, S., Ziyaei, E., Rasooli, A., & Hosseinpour, S. (2019). Characterization of pulse and direct current methods for electrodeposition of Ni-Co composite coatings reinforced with nano and micro ZnO particles. Metallurgical and Materials Transactions A, 50, 1922-1935. https://doi.org/10.1007/s11661-019-05118-y
44. Sajjadnejad, M., Haghshenas, S. M. S., Badr, P., Setoudeh, N., & Hosseinpour, S. (2021). Wear and tribological characterization of nickel matrix electrodeposited composites: A review. Wear, 486, 204098. https://doi.org/10.1016/j.wear.2021.204098
45. Dehgahi, S., Amini, R., & Alizadeh, M. (2016). Corrosion, passivation and wear behaviors of electrodeposited Ni–Al2O3–SiC nano-composite coatings. Surface and Coatings Technology, 304, 502-511. https://doi.org/10.1016/j.surfcoat.2016.07.007
46. Thiemig, D., & Bund, A. (2009). Influence of ethanol on the electrocodeposition of Ni/Al2O3 nanocomposite films. Applied Surface Science, 255(7), 4164-4170. https://doi.org/10.1016/j.apsusc.2008.10.114
47. Tabakovic, I., & Venkatasamy, V. (2018). Preparation of metastable CoFeNi alloys with ultra-high magnetic saturation (Bs= 2.4–2.59 T) by reverse pulse electrodeposition. Journal of Magnetism and Magnetic Materials, 452, 306-314. https://doi.org/10.1016/j.jmmm.2017.12.003
48. Yar-Mukhamedova, G., Sakhnenko, N., & Nenastina, T. (2018). Electrodeposition and properties of binary and ternary cobalt alloys with molybdenum and tungsten. Applied Surface Science, 445, 298-307. https://doi.org/10.1016/j.apsusc.2018.03.171
49. Li, B., Zhang, W., Zhang, W., & Huan, Y. (2017). Preparation of Ni-W/SiC nanocomposite coatings by electrochemical deposition. Journal of Alloys and compounds, 702, 38-50. https://doi.org/10.1016/j.jallcom.2017.01.239
50. Frade, T., Bouzon, V., Gomes, A., & da Silva Pereira, M. I. (2010). Pulsed-reverse current electrodeposition of Zn and Zn-TiO2 nanocomposite films. Surface and Coatings Technology, 204(21-22), 3592-3598. https://doi.org/10.1016/j.surfcoat.2010.04.030
51. Chandrasekar, M. S., & Pushpavanam, M. (2008). Pulse and pulse reverse plating—Conceptual, advantages and applications. Electrochimica Acta, 53(8), 3313-3322. https://doi.org/10.1016/j.electacta.2007.11.054
52. Yang, Y., & Cheng, Y. F. (2013). Fabrication of Ni–Co–SiC composite coatings by pulse electrodeposition—Effects of duty cycle and pulse frequency. Surface and Coatings Technology, 216, 282-288. https://doi.org/10.1016/j.surfcoat.2012.11.059
53. Bai, Q., Zhang, L., Ke, L., Zhu, P., Ma, Y., Xia, S., & Zhou, B. (2020). The effects of surface chemical treatment on the corrosion behavior of an Al-B4C metal matrix composite in boric acid solutions at different temperatures. Corrosion Science, 164, 108356. https://doi.org/10.1016/j.corsci.2019.108356
54. Clinktan, R., Ramkumar, K. R., & Sivasankaran, S. (2020). Effect of boron carbide addition on strengthening mechanisms, cold workability and instantaneous strain hardening behaviour of Cu4Si14Zn nanocomposites. Materials Science and Engineering: A, 787, 139538. https://doi.org/10.1016/j.msea.2020.139538
55. Ramadoss, N., Pazhanivel, K., Ganeshkumar, A., & Arivanandhan, M. (2023). Microstructural, mechanical and corrosion behaviour of B4C/BN-reinforced Al7075 matrix hybrid composites. International Journal of Metalcasting, 17(1), 499-514. https://doi.org/10.1007/s40962-022-00791-z
56. Rezagholizadeh, M., Ghaderi, M., Heidary, A., & Monirvaghefi, S. M. (2015). The effect of B 4 C nanoparticles on the corrosion and tribological behavior of electroless Ni-BB 4 C composite coatings. Surface engineering and applied electrochemistry, 51, 18-24. https://doi.org/10.3103/S1068375515010135

57. Pushpanathan, D. P., Alagumurthi, N., & Devaneyan, S. P. (2020). On the microstructure and tribological properties of pulse electrodeposited Ni-B4C-TiC nano composite coating on AZ80 magnesium alloy. Surfaces and Interfaces, 19, 100465. https://doi.org/10.1016/j.surfin.2020.100465
58. Dong, S., Yang, Y., Liang, T., Ma, R., Du, A., Yang, M., Fan, Y., Zhao, Z., & Cao, X. (2021). Construction and corrosion resistance of Ni-B4C superhydrophobic composite coatings on Q235 steel. Surface and Coatings Technology, 422, 127551. https://doi.org/10.1016/j.surfcoat.2021.127551
59. Li, H., He, Y., Luo, P., Fan, Y., Yu, H., Wang, Y., He, T., Li, Z., & Zhang, H. (2021). Influence of pulse frequency on corrosion resistance and mechanical properties of Ni-W/B4C composite coatings. Colloids and Surfaces A: Physicochemical and Engineering Aspects, 629, 127436. https://doi.org/10.1016/j.colsurfa.2021.127436
60. Venses, G., Sivapragash, M., Kumar, T. S., & Rex, F. M. T. (2022). Optimisation of Corrosion behaviour and hardness of Ni-B4C Composite coated AZ31 Mg alloy using RSM. Surface Topography: Metrology and Properties, 10(1), 015033. https://doi.org/10.1088/2051-672X/ac577f
61. Baghal, S. L., Amadeh, A., Sohi, M. H., & Hadavi, S. M. M. (2013). The effect of SDS surfactant on tensile properties of electrodeposited Ni–Co/SiC nanocomposites. Materials Science and Engineering: A, 559, 583-590. https://doi.org/10.1016/j.msea.2012.08.145
62. Mosayebi, S., Rezaei, M., & Mahidashti, Z. (2020). Comparing corrosion behavior of Ni and Ni-Mo electroplated coatings in chloride mediums. Colloids and Surfaces A: Physicochemical and Engineering Aspects, 594, 124654. https://doi.org/10.1016/j.colsurfa.2020.124654
63. Razaghi, Z., Rezaei, M., & Tabaian, S. H. (2020). Electrochemical noise and impedance study on the corrosion of electroplated Ni-Cr coatings in HBF4 aqueous solution. Journal of Electroanalytical Chemistry, 859, 113838. https://doi.org/10.1016/j.jelechem.2020.113838
64. Surender, M., Balasubramaniam, R., & Basu, B. (2004). Electrochemical behavior of electrodeposited Ni–WC composite coatings. Surface and Coatings Technology, 187(1), 93-97. https://doi.org/10.1016/j.surfcoat.2004.01.030
65. [65] Baghery, P., Farzam, M., Mousavi, A. B., & Hosseini, M. (2010). Ni–TiO2 nanocomposite coating with high resistance to corrosion and wear. Surface and Coatings Technology, 204(23), 3804-3810. https://doi.org/10.1016/j.surfcoat.2010.04.061
66. Dini, J. W. (1998). The materials science of coatings and substrates. Metal Finishing, 50, 47. https://www.researchgate.net/profile/Zainab-Raheem-2/publication/334737122_ELECTRODEPOSITION_The_Materials_Science_of_Coatings_and_Substrates/links/5d3eaf514585153e592ab1ea/ELECTRODEPOSITION-The-Materials-Science-of-Coatings-and-Substrates.pdf
67. Ebrahimi, F., & Ahmed, Z. (2003). The effect of current density on properties of electrodeposited nanocrystalline nickel. Journal of Applied Electrochemistry, 33, 733-739. https://doi.org/10.1023/A:1025049802635
68. Rashidi, A. M., & Amadeh, A. (2010). Effect of electroplating parameters on microstructure of nanocrystalline nickel coatings. Journal of Materials Science & Technology, 26(1), 82-86. https://doi.org/10.1016/S1005-0302(10)60013-8
69. Chen, L., Wang, L., Zeng, Z., & Xu, T. (2006). Influence of pulse frequency on the microstructure and wear resistance of electrodeposited Ni–Al2O3 composite coatings. Surface and Coatings Technology, 201(3-4), 599-605. https://doi.org/10.1016/j.surfcoat.2005.12.008
70. Lajevardi, S. A., & Shahrabi, T. (2010). Effects of pulse electrodeposition parameters on the properties of Ni–TiO2 nanocomposite coatings. Applied Surface Science, 256(22), 6775-6781. https://doi.org/10.1016/j.apsusc.2010.04.088
71. Badr, P., Sajjadnejad, M., & Haghshenas, S. M. S. (2023). Influence of Incorporating B4C Nanoparticles and Pulse Electrodeposition Parameters on the Surface Morphology and Wear Behavior of Nickel Based Nanocomposite Coatings. *Progress in Chemical and Biochemical Research*, *6*(4), 292-313. https://doi.org/10.22034/pcbr.2023.394780.1261
72. Mustapha, S., Ndamitso, M. M., Abdulkareem, A. S., Tijani, J. O., Shuaib, D. T., Mohammed, A. K., & Sumaila, A. (2019). Comparative study of crystallite size using Williamson-Hall and Debye-Scherrer plots for ZnO nanoparticles. Advances in Natural Sciences: Nanoscience and Nanotechnology, 10(4), 045013. https://doi.org/10.1088/2043-6254/ab52f7
73. Li, B., Mei, T., Chu, H., Wang, J., Du, S., Miao, Y., & Zhang, W. (2021). Ultrasonic-assisted electrodeposition of Ni/diamond composite coatings and its structure and electrochemical properties. Ultrasonics Sonochemistry, 73, 105475. https://doi.org/10.1016/j.ultsonch.2021.105475
74. Tao, Y., Ma, F., Teng, M., Jia, Z., & Zeng, Z. (2019). Designed fabrication of super high hardness Ni-B-Sc nanocomposite coating for anti-wear application. Applied Surface Science, 492, 426-434. https://doi.org/10.1016/j.apsusc.2019.06.233
75. Amadeh, A., Rahimi, A., Farshchian, B., & Moradi, H. (2010). Corrosion behavior of pulse electrodeposited nanostructure Ni–SiC composite coatings. Journal of Nanoscience and Nanotechnology, 10(8), 5383-5388. https://doi.org/10.1166/jnn.2010.1931
76. Medelien, V. (2002). The influence of B4C and SiC additions on the morphological, physical, chemical and corrosion properties of Ni coatings. Surface and coatings Technology, 154(1), 104-111. https://doi.org/10.1016/S0257-8972(01)01703-0
77. Jiang, J. B., Liu, W. D., Zhang, L., Zhong, Q. D., Wang, Y., & Zhou, Q. Y. (2012). Electrodeposition and hardness and corrosion resistance propertie of Ni/nano-B4C composite coatings. Advanced Materials Research, 399, 2055-2060. https://doi.org/10.4028/www.scientific.net/AMR.399-401.2055
78. Omidvar, H., Sajjadnejad, M., Stremsdoerfer, G., Meas, Y., & Mozafari, A. (2015). Characterization of NiBP-graphite composite coatings deposited by dynamic chemical plating. Anti-Corrosion Methods and Materials, 62(2), 116-122. https://doi.org/10.1108/ACMM-11-2013-1320
79. Javidi, M., Haghshenas, S. M. S., & Shariat, M. H. (2020). CO2 corrosion behavior of sensitized 304 and 316 austenitic stainless steels in 3.5 wt.% NaCl solution and presence of H2S. Corrosion Science, 163, 108230. https://doi.org/10.1016/j.corsci.2019.108230